Electromagnetic wave absorption performance of UHPC incorporated with carbon black and carbon fibre

[1]Shenchun Xu, [2]Yekai Yang, [3*]Chengqing Wu
[1]Protective structures centre, Guangzhou University, Guangzhou 510006, China
[2]School of Civil Engineering, Tianjin University, Tianjin 300372, China
[3]School of Civil and Environmental Engineering, University of Technology Sydney, NSW 2007, Australia

Abstract: This study focuses on the electromagnetic wave absorption performance (EWAP) of ultra-high-performance concrete (UHPC) incorporated with carbon black (CB) and carbon fiber (CF) in 2-18 GHz frequency range (required for the radar wave absorbing materials). The reflectivity of the traditional UHPC was investigated and compared with the cement-based composites reported in literatures, so as to illustrate the advantages of novel UHPCs with respect to EWAP. Afterwards, the effect of CB and CF on the compressive strength, complex permittivity and reflectivity of the novel UHPCs was investigated. The microstructure of the novel UHPCs was also explored via scanning electron microscopy to illustrate the mechanism of performance enhancement on incorporating CB and CF. The results indicated that EWAP of the traditional UHPC was similar or inferior (at specific frequencies) to the literature reported cement-based composites. However, EWAP of the novel UHPCs was significantly improved after reinforcing with CB or CF. A positive effect of CB and CF was also observed on the compressive strength of the developed UHPCs. This study provides avenues for the use of UHPCs in protecting structures for absorbing the electromagnetic waves and safeguarding these structures against extreme loads, including blast and penetration.

Keywords: electromagnetic wave absorption performance; UHPC; carbon black; carbon fiber; compressive strength.

1. Introduction

The stringent technical requirements are put forward for the protective engineering structures owing to the rapid development of the modern military technology. It requires that the protective engineering structures are not only resistant to blast/penetration but are also non-detectable [1]. Considerable achievements have been made in improving blast/penetration resistance of the protective structures, such as the application of the composite materials. Roller et al. [2] revealed the superiority of hardening or retrofitting with high-performance materials for improving the blast resistance of the RC columns. Ha et al. [3] reported that the hybrid CFRP-PU composite led a superior improvement in the blast resistance of a RC slab as compared to the ordinary retrofitted fibre reinforced polymers. In another study, Yammaguchi et al. [4] concluded that an air cavity created between the two layers of a polyethylene fiber reinforced concrete slab effectively reduced the spall damage under contact blast. Among the composite materials, ultra-high-performance concrete (UHPC) represents an innovative cementitious material and possesses extraordinary characteristics, such as excellent strength, energy absorption capacity, durability and workability [5-9]. Consequently, the superiority of UHPC in improving the blast/penetration resistance of the RC structures has been proved by many literature studies. Wu et al. [10] carried out a series of investigations to explore the blast resistance of the UHPC structural elements, and the performance of UHPC was concluded to be significantly superior than the conventional concrete. Liu et al. [11-13] revealed the improved penetration resistance of the engineering structures incorporating UHPC. Likewise, Wu et al. [14] confirmed the superior penetration resistance of UHPC against an impact loading at a high velocity in the range 510-1320 m/s.

Similarly, investigations on the electromagnetic wave absorption performance (EWAP) of the cement-based materials have been carried out to enhance the non-detectability of the protective structures as well as to reduce the electromagnetic pollution harmful to the humans and electronic equipment. Wang et al. [15] employed expanded perlite as an electromagnetic emission aggregate to optimize the impedance matching of the cement-based composites. In the 2-18 GHz frequency range, the absorption bandwidth with < -10 dB reflectivity was achieved at 14 GHz. Zhang et al. [16] studied the effect and corresponding mechanism of multi-walled carbon nanotubes on EWAP of the cement-based

composites. The carbon nanotubes were observed to improve the electromagnetic properties of the composites. Li et al. [17] also reported that nano-TiO_2 affected EWAP of the cement-based composites through the dielectric loss, rather than the magnetic loss.

Overall, researchers have separately studied the mechanical properties of UHPC and EWAP of the cement-based materials. However, the mechanical properties of the cement-based composites reported in literatures are not optimal to resist the blast or penetration loading. On the other hand, the studies on EWAP of UHPC are also limited. Therefore, it is vital to develop novel UHPCs with a combination of excellent mechanical properties and EWAP so to effectively protect the critical engineering structures.

In general, a functional strategy to improve EWAP of the cement-based materials is to introduce the dielectric or magnetic loss fillers [18], such as carbonaceous materials [19-22], ferrites [23,24], metal powders [25] and industrial by-products [26]. A number of studies have been carried out to investigate the effect of the carbonaceous materials on the mechanical or electromagnetic wave absorption performance of the cement-based composites, owing to their beneficial characteristics, such as abundant sources, low density and high conductivity [27]. Among these, carbon black (CB), a low-cost carbonaceous material, has been widely used in the rubber, plastic and other industries. It has been widely reported that the incorporation of CB can remarkably improve the dielectric constant and loss factor of the cement-based materials [28,29]. Moreover, it is also an effective admixture for improving the workability of the cement-based materials [30]. Further, carbon fiber (CF) is another novel carbonaceous material with high conductivity, which has been reported to be effective in improving the electromagnetic wave absorption capacity and effective bandwidth [18]. The "effective bandwidth" is a critical index to estimate the reflectivity of the material, which refers to the sum of all frequency ranges with reflectivity less than -10 dB. The greater the effective bandwidth, the wider absorption range of the material.

However, the effect of CF or CB on the EWAP and mechanical properties of UHPC was still limited. Based on this, the current study developed novel UHPCs incorporated with CB and CF. Meanwhile, the main mechanical properties and EWAP of the novel UHPCs in the 2-18 GHz frequency range (required for the radar wave absorption materials; common radar waves are mainly distributed in this frequency band) were investigated in detail. A series of compression, coaxial probe and arch tests were

carried out to investigate the effect of CB and CF on the compressive strength, complex permittivity and reflectivity of UHPC. The scanning electron microscopy (SEM) analysis was performed to reveal the mechanism of performance enhancement on incorporating CB and CF. Furthermore, the effectiveness of CB and CF in improving EWAP of UHPC was also compared. The compressive strength and reflectivity of the UHPC materials developed in this study were also compared with the cement-based composites reported in literatures. This study would promote the application of the developed novel UHPCs with superior mechanical properties and excellent EWAP in the field of the protective structures. The survivability of the critical engineering structures could also be further improved.

2. Electromagnetic wave absorption theory for a single-layer plate

Fig. 1 presents the mechanism of interaction of the electromagnetic wave with the corresponding medium. After interaction, the incident wave is transformed into three components, including reflected, transmitted and absorbed waves. Correspondingly, the reflection coefficient ***r***, absorption coefficient ***a*** and transmission coefficient ***t*** present the following relationship [31,32]:

$$r + a + t = 1 \tag{1}$$

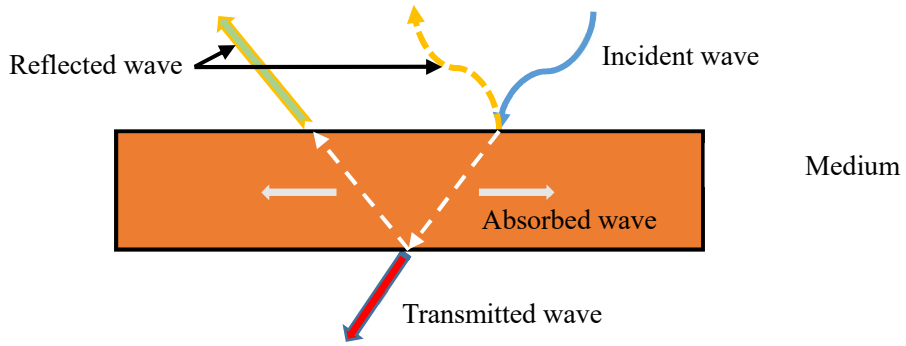

Fig. 1. The propagation path of the electromagnetic wave.

To reduce the detectability of the protective structures, the electromagnetic wave absorption materials should be exploited in the construction. For designing such materials, the incident electromagnetic wave is expected to either be absorbed during propagation through the absorbing material or pass through the material without any significant reflection on the interface [33,34]. This requires the absorption material to possess the attenuation and impedance matching characteristics [35].

The design of the impedance matching characteristic refers to the creation of specific boundary conditions to minimize the reflection coefficient r (which is zero for the ideal case). As per the

electromagnetic theory [36,37], the reflection coefficient r satisfies the following relationship as the incident electromagnetic wave propagates vertically through the medium.

$$r = \frac{Z - Z_0}{Z + Z_0} \tag{2}$$

where Z is the input impedance of the material, and Z_0 is the free space wave impedance (377 Ω).

The input impedance (Z_{in}) of a single-layer medium with a reflective backing can be expressed as [38]:

$$Z_{in} = Z_c \tanh(\gamma \cdot d) \tag{3}$$

$$Z_c = \sqrt{\frac{\mu_r}{\varepsilon_r}} \tag{4}$$

$$\gamma = \frac{j2\pi f \sqrt{\mu_r \varepsilon_r}}{c} \tag{5}$$

where Z_c is the characteristic impedance; γ is the propagation constant; d is the thickness of the medium; j is the imaginary number; ε_r is the complex permittivity; μ_r is the complex permeability; f is the electromagnetic wave frequency, and c is the propagation velocity of the electromagnetic wave in vacuum. Therefore, the reflection coefficient r of a single-layer medium with a reflective backing can be derived by substituting Eqs. (3)-(5) in Eq. (2), as follows:

$$r = \frac{\sqrt{\frac{\mu_r}{\varepsilon_r}} \tanh\left(j\frac{2\pi f}{c}\sqrt{\mu_r \varepsilon_r} d\right) - 1}{\sqrt{\frac{\mu_r}{\varepsilon_r}} \tanh\left(j\frac{2\pi f}{c}\sqrt{\mu_r \varepsilon_r} d\right) + 1} \tag{6}$$

Further, the attenuation characteristic refers to the effective absorption and attenuation of the incident electromagnetic wave [39,40]. It is attributed to the electromagnetic loss, i.e., the electromagnetic wave energy is transformed into other forms of energy, such as heat. Generally, the loss tangent (tan(δ)) is used to reflect the capability of the medium to absorb/attenuate the electromagnetic wave. Further, it can be classified as the dielectric loss (tan(δ_E)) and magnetic loss (tan(δ_M)) tangent, as shown in the following equations:

$$\tan(\delta_E) = \varepsilon'' / \varepsilon' \tag{7}$$

$$\tan(\delta_M) = \mu'' / \mu' \tag{8}$$

where, ε' and ε'' are the real and imaginary parts of the complex permittivity ($\varepsilon_r = \varepsilon' - j\varepsilon''$), respectively,

and μ' and μ'' are the real and imaginary parts of the complex permeability ($\mu_r=\mu' - j\mu''$), respectively.

However, it should be noted that the magnetic loss was ignored in this study as the developed materials were non-magnetic. Correspondingly, Eq. (6) was simplified by solely considering the dielectric loss, as follows:

$$r = \frac{\sqrt{\frac{1}{\varepsilon_r}}\tanh\left(j\frac{2\pi f}{c}\sqrt{\varepsilon_r}d\right)-1}{\sqrt{\frac{1}{\varepsilon_r}}\tanh\left(j\frac{2\pi f}{c}\sqrt{\varepsilon_r}d\right)+1} \tag{9}$$

Eventually, the reflectivity R can be expressed as:

$$R = 20\lg|r| \tag{10}$$

3. Experiment

3.1 Materials

The traditional UHPC investigated in this study was fabricated by using cement, silica fume, fly ash, quartz sand and nanoparticles (Nano-CaO). Portland cement with a 28-day nominal compressive strength of 52.5 MPa was used as the binder material. Silica fume was added to the mixture as a supplementary cementitious material owing to its excellent pozzolanic activity and micro-aggregation effect, which improve the microstructure of the hardened cement paste. Moreover, fly ash reinforced with micro-spheres was incorporated in the mixture to improve the internal microstructure and interfacial properties. Further, the addition of fly ash reduces the heat of hydration and improves the workability and compactness of concrete, along with decreasing the environmental pollution. The nanoparticles (Nano-CaO) were chosen to further ensure the compactness of concrete, along with reducing the internal defects. Quartz sand with a particle size in the range 106-850 μm was used as the fine aggregate. Based on the particle size, it was divided into three fractions: coarse (380-830 μm), medium (212-380 μm) and fine (125-212 μm) sand. The required workability was achieved by the addition of polycarboxylic type superplasticizer and water. The composition of the traditional UHPC is presented in Table 1.

Table 1. The composition of UHPC (unit: kg/m^3)

P.O. 52.5 Cement	Silica fume	Fly ash	Quartz sand	Nano-CaO	Superplasticizer	Water

700	150	125	1040	21.72	16	190

Further, CB (Fig. 2(a)) or CF (Fig. 2(b)) was added to the formulation of the traditional UHPC. K70 conductive CB meeting the Chinese Standard GB 3778-2011 was used, and its main characteristics are presented in Table 2. The average particle size of CB was 13 μm, with resistivity < 2.5 Ω·m. Straight CF with 6 mm length and 7 μm diameter was used in this study. Its main features are listed in Table 3. As observed, CF possessed super high strength (4900 MPa) and Young's modulus (240 GPa). Additionally, the resistivity of CF was 0.15 Ω·m, thus, indicating a superior conductivity.

(a) Carbon black (b) Carbon fiber

Fig. 2. Images of (a) carbon black and (b) carbon fiber.

Table 2. Properties of carbon black

Resistivity (Ω·m)	Particle size (μm)	DBP (ml/100g)	Lodine adsorption number (mg/g)
<2.5	13	150-170	85-100

Table 3. Properties of carbon fiber

Resistivity (Ω·m)	Length (mm)	Diameter (μm)	Strength (MPa)	Young's modulus (GPa)
0.15	6	7	4900	240

3.2 Design and fabrication of specimens

The mixing process of the traditional UHPC was achieved in three stages based on the mixture design: (a) the mixture containing cement, silica fume, nanoparticles and fly ash was first mixed for 5 minutes; (b) quartz sand was subsequently added to the mixture and mixed for further 2 minutes; (c) superplasticizer and water were poured in the mixture and mixed for additional 5 minutes. For generating UHPC with CB or CF, the CB or CF filler was added prior to pouring the mixture of superplasticizer and water, and the contents were mixed for 5 minutes. After completing the mixing

process, the final mixtures were poured in the molds, followed by curing at room temperature for 24 h. Subsequently, the hardened UHPC samples were removed from the molds and cured in water at 90 ℃ for additional 48 h. Eventually, the developed novel UHPCs were naturally cured at room temperature until characterization.

In order to investigate the effect of CB and CF on EWAP of UHPC, the volume fraction of CB was varied as 1.3%, 2.0% and 2.7%, whereas the volume fraction of CF was varied as 0.1%, 0.3% and 0.5%. Here, it should be pointed out that the UHPC incorporated with CF was very hard to mix when the volume ratio of CF exceeded 1.0 %. Therefore, a relatively low volume ratio of CF was adopted in this study. CB did not have such a problem, however, its volumetric ratio effect on the UHPC reflectivity could be not easily observed when the same proportion increase was adopted. Hence, the increment in different volumetric ratios for both materials was adopted in this study. To carry out the characterization, two types of test specimens were designed based on the Chinese Standards GB/T 50081-2019 and GJB 2038A-2011. The cubic specimens with dimensions of 100 mm × 100 mm × 100 mm were used for the characterization of permittivity and compressive strength. On the other hand, the dimensions of the specimens for the reflectivity tests were 200 mm × 200 mm × 20 mm. Three identical specimens were tested for each specimen type to ensure the accuracy and reliability of the test data (a total of 63 specimens were tested) and the average value of the three identical specimens was adopted. The details of the tested samples are presented in Table 4. In this table, specimens have been classified based on the variable to be investigated, type of UHPC, dosage of the variable and test type. In the composite notation, N refers to traditional; CB refers to carbon black; CF refers to carbon fiber; UHPC-X refers to ultra-high-performance concrete followed by the dosage of the variable (X); Perm refers to the permittivity test; Refl refers to the reflectivity test, and CST refers to the compressive strength test. For instance, the specimen CB-UHPC-1.3-Perm indicates that this UHPC specimen was mixed with 1.3 vol.% carbon black, and it was tested for permittivity. Here, it should be noted that "vol.%" was used in following sections to express the volumetric ratio of CB or CF.

Table 4. Test matrix

Specimen code	Filler type	Volume ratio (%)	Test type
N-UHPC-CST	---	---	CST
N-UHPC-Perm			Perm

N-UHPC-Refl			Refl
CB-UHPC-1.3-CST			CST
CB-UHPC-1.3-Perm		1.3	Perm
CB-UHPC-1.3-Refl			Refl
CB-UHPC-2.0-CST			CST
CB-UHPC-2.0-Perm	CB	2.0	Perm
CB-UHPC-2.0-Refl			Refl
CB-UHPC-2.7-CST			CST
CB-UHPC-2.7-Perm		2.7	Perm
CB-UHPC-2.7-Refl			Refl
CF-UHPC-0.1-CST			CST
CF-UHPC-0.1-Perm		0.1	Perm
CF-UHPC-0.1-Refl			Refl
CF-UHPC-0.3-CST			CST
CF-UHPC-0.3-Perm	CF	0.3	Perm
CF-UHPC-0.3-Refl			Refl
CF-UHPC-0.5-CST			CST
CF-UHPC-0.5-Perm		0.5	Perm
CF-UHPC-0.5-Refl			Refl

3.3 Test setup

3.3.1 Compressive strength

The test setup for analyzing the compressive strength is shown in Fig. 3. A hydraulic testing machine was used at a load of 3000 kN. Both force-controlled and displacement-controlled loading stages were employed. First, a compressive load of 50 kN (predicted) was applied on the specimen to stabilize the equipment and eliminate the clearance between the specimen and loader. Subsequently, the displacement-controlled loading was applied on the specimen at a loading rate of 0.2 mm/min until the specimen failed. Two LVDTs were positioned to continuously monitor the axial deformation of the specimen.

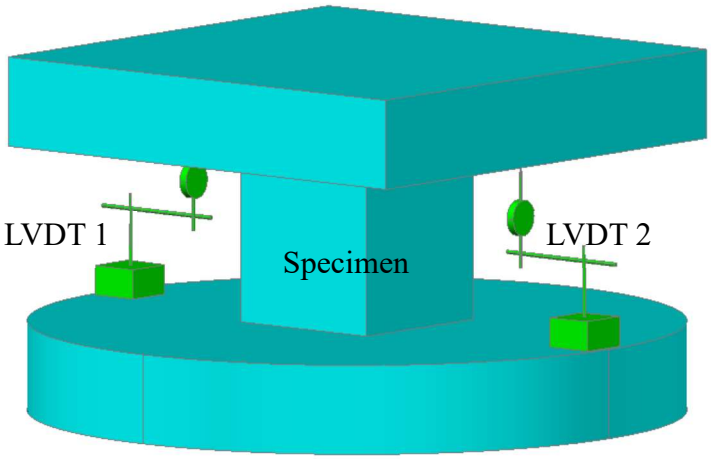

Fig. 3. Schematic diagram of the compression test setup.

3.3.2 Permittivity

In general, the electromagnetic waves can be dissipated via the electrical and magnetic losses of the material. However, the UHPC composites investigated in this study were treated as the electrical loss materials owing to the non-magnetic components, and the corresponding magnetic loss can be ignored. Therefore, the complex permittivity of UHPC was characterized via the coaxial probe method to reveal the effect of CB and CF on the electrical loss of UHPC, as shown in Fig. 4. The test system included a vector network analyzer, a Keysight 85070 series dielectric probe kit and a support. The specimen was placed on the support prior to the test. Afterwards, the probe was placed on the surface of the specimen to determine the complex permittivity in 2-18 GHz frequency range. The test procedure was non-destructive and was conducted in real-time. All six surfaces of the specimen were tested, and the average value was reported.

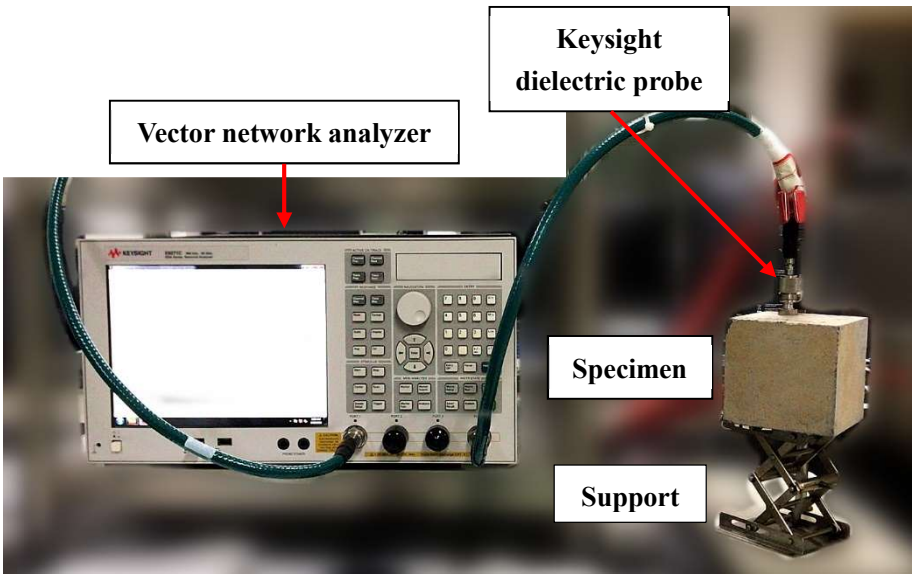

Fig. 4. Setup of the permittivity test.

Further, the real part of the complex permittivity is known as the dielectric constant, which represents the impedance matching characteristic. On the other hand, the imaginary part is termed as the loss factor, which reflects the dielectric loss in the electromagnetic wave absorption theory [22]. As per the coaxial probe method, the impedance of the target is determined based on the real part of the complex permittivity in order to analyze the effect on the impedance matching characteristic, as shown in Eq. (11). In addition, the power loss per unit volume in the medium is proportional to the imaginary part based on the electromagnetic wave theory, as shown in Eq. (12), in which w_e is the power loss per unit volume, ω is the angular frequency, and E is the amplitude.

$$Z = \frac{Z_0}{\sqrt{\varepsilon'}} \tag{11}$$

$$w_e = \frac{1}{2}\omega\varepsilon'' E^2 \tag{12}$$

3.3.3 Reflectivity

The reflectivity is the ultimate index to evaluate EWAP of the medium. The arch test method was used to reveal the reflectivity of UHPC in 2-18 GHz frequency range based on the Chinese Standard GJB2038A-2001. As shown in Fig. 5, the test system consisted of two antennas, an arch frame, a vector network analyzer, a high-performance electromagnetic wave absorbing material (HPEWAM), a specimen holder and a reflective backing. Prior to testing, the specimen was placed on the specimen holder located on a table, and the reflective backing was achieved through the table. During testing, one of the antennas transmits the electromagnetic wave to the specimen, and the other antenna receives the reflected electromagnetic wave. HPEWAM was used to absorb the redundant electromagnetic wave signals so as to eliminate interference.

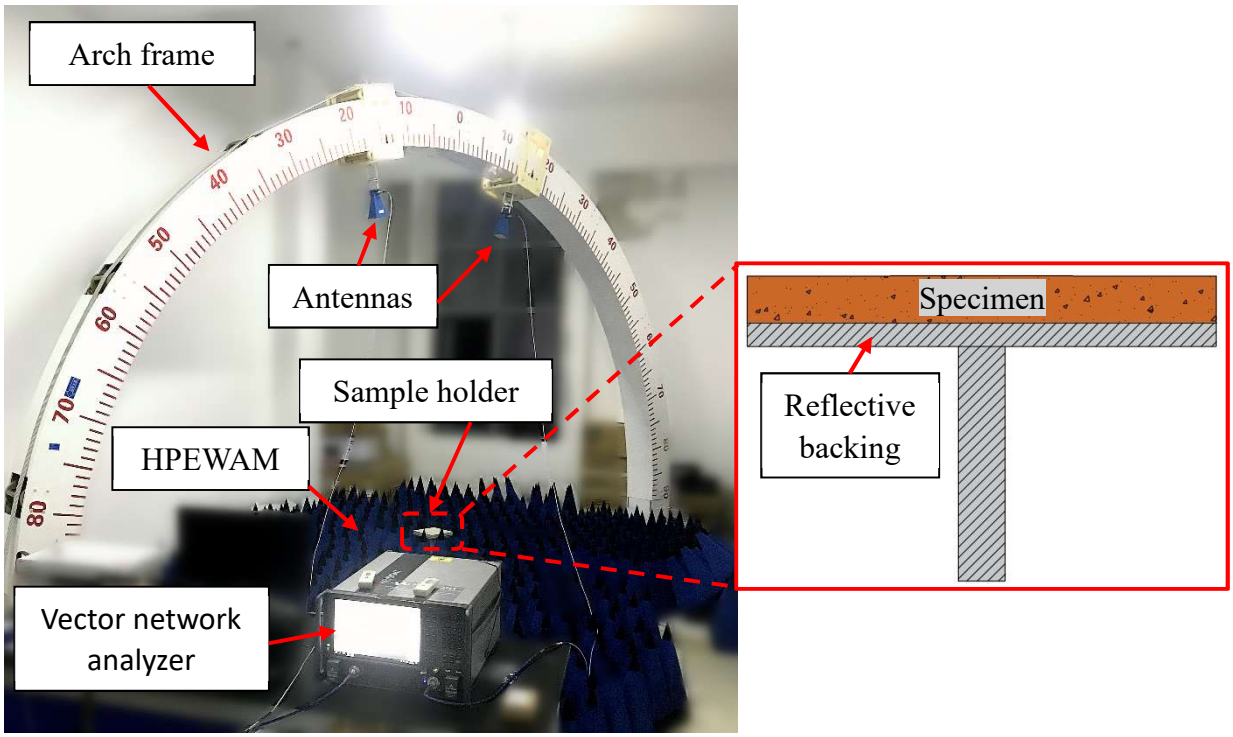

Fig. 5. Setup of the reflectivity test.

4. Results

4.1 Compressive strength and reflectivity of traditional UHPC

The compressive strength and reflectivity of the traditional UHPC were first investigated. The average compressive strength was determined to be 116.3 MPa, which was much higher than that of the cement-based composites reported in literature [18,20,41].

Furthermore, the reflectivity of UHPC in 2-18 GHz frequency range is shown in Fig. 6. The reflectivity presented a small vibration around -7.5 dB in 2-11.8 GHz frequency range (thus, the value was above -10 dB). As the frequency exceeded 11.8 GHz, the reflectivity presented a large vibration. Specifically, a dramatic decrease was observed from -5.1 dB to -12 dB in 11.8 - 12.5 GHz frequency range. Subsequently, the reflectivity increased to -6.2 dB as the frequency reached 15 GHz, followed by a decline to the minimum value (-13.76 dB) at 18 GHz. Correspondingly, the bandwidth with reflectivity < -10 dB was 0.80 GHz. For reference, the relationship between the reflectivity and frequency of the literature reported cement-based composites [18,20,41] is also plotted in Fig. 6. As observed, the pure cement in reference [18] exhibited the strongest absorption peak at 3.8 GHz with a reflectivity of -13 dB. Further, an additional absorption peak was located at 6 GHz with a reflectivity of -11 dB. Correspondingly, the effective bandwidth with reflectivity below -10 dB was 1 GHz. The cement-

based composite in reference [20] presented the strongest absorption peak at 2.9 GHz with a reflectivity of -22 dB. In addition, two absorption signals were observed between 4 and 8 GHz with an approximate reflectivity of -12 dB. Correspondingly, the effective bandwidth with reflectivity below -10 dB was 1 GHz. Moreover, the pure cement in reference [41] demonstrated the strongest absorption peak at 3.9 GHz with a reflectivity of -10.8 dB, and the corresponding effective bandwidth with reflectivity below -10 dB was close to 2 GHz.

By comparison, the effective bandwidth of the traditional UHPC tested in this experiment is observed to be significantly less than or close to that of the other cement-based composites. Thus, it indicated that EWAP of the traditional UHPC was similar or inferior (at specific frequencies) to the other cement-based composites. To gain further insights, the microstructure of UHPC was investigated by SEM, as shown in Fig. 7. A highly compact microstructure was observed to be formed by the C-S-H gel. Further, the impedance matching between the air space and UHPC was deteriorated by the highly compact microstructure [42]. Correspondingly, it was increasingly difficult for the electromagnetic wave to enter the concrete sample, leading to an enhanced reflectivity.

Overall, it can be suggested that the traditional UHPC investigated in this study possesses significantly high compressive strength, however, it is vital to improve its EWAP to reduce the detectability of the engineering structures, along with enhancing their safety.

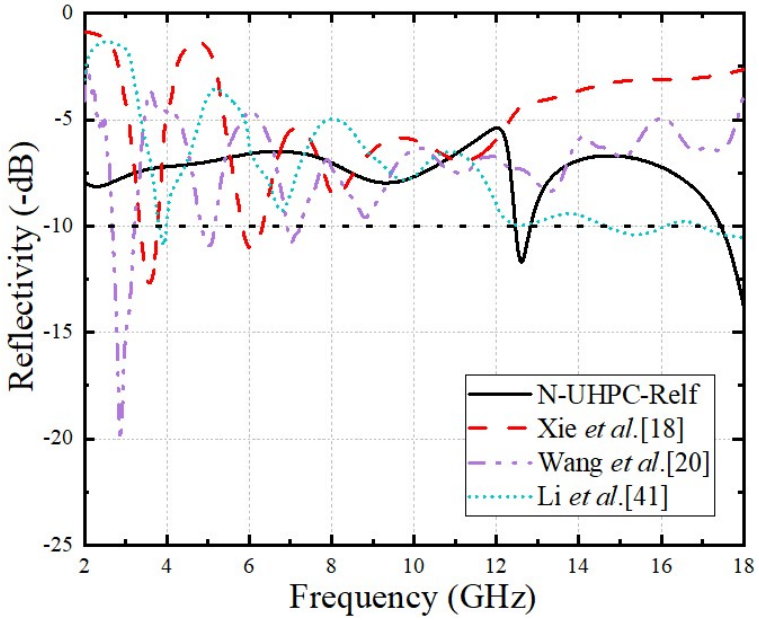

Fig. 6. The comparison of the reflectivity of the traditional UHPC with the literature reported cement-based composites.

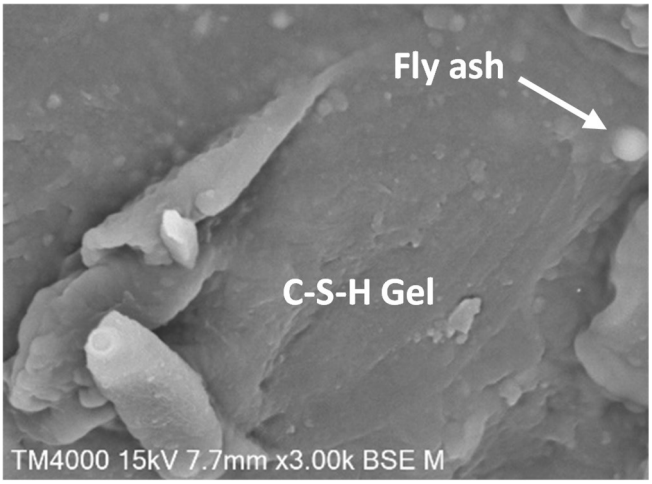

Fig. 7. The SEM micrograph of the traditional UHPC.

4.2 Effect of carbon black and carbon fiber on permittivity of UHPCs

4.2.1 Effect of Carbon black

The complex permittivity of UHPCs was characterized by using the coaxial probe method, and the dielectric loss tangent was derived based on Eq. (9). As mentioned earlier, the real part of the complex permittivity is referred to as the dielectric constant, which represents the impedance matching characteristic. On the other hand, the imaginary part is defined as the loss factor, which reflects the dielectric loss in the electromagnetic wave absorption theory [22]. Therefore, the effect of CB and CF on the real and imaginary parts of the complex permittivity was analyzed. Fig. 8 shows the effect of CB on the complex permittivity of UHPCs. For comparison, the complex permittivity of the traditional UHPC is also plotted in Fig. 8.

The effect of CB on the real part of the complex permittivity is shown in Fig. 8(a). The real part of the complex permittivity of UHPCs initially presented a plateau stage, followed by a significant decrease. The real part of the complex permittivity of the traditional UHPC and CB-UHPC-1.3-Prem decreased from the 4.6 and 4.4 (plateau value in 2-4 GHz frequency range) to 3.6 and 3.2 (the minimum at 12 GHz). Afterwards, a slight increase was observed till 18 GHz. The real part of the complex permittivity for CB-UHPC-2.0-Perm and CB-UHPC-2.7-Perm exhibited a continuous decline after the plateau stage without any increase. The value of the real part of the complex permittivity for CB-UHPC-2.0-Perm and CB-UHPC-2.7-Perm in the plateau stage was 4.6 and 5.3, respectively (in 2-5 GHz frequency range). At 18 GHz, the permittivity for the two composites gradually decreased to 3.8 and 4.1, respectively. Thus, the real part of the complex permittivity of UHPC with 1.3 vol.% CB was noted to

be smaller than that of the traditional UHPC in 2-18 GHz frequency range. On the other hand, its value for UHPC with 2.0 vol.% CB was close to that of the traditional UHPC in 2-5 GHz frequency range, where the value was higher in 5-18 GHz frequency range. On further enhancing the CB content to 2.7 vol.%, the real part of the complex permittivity demonstrated the highest values in the full frequency range of 2-18 GHz. This was because the low content of CB (1.3 vol.%) altered the microstructure of UHPC, which resulted in the increase in the resistance of UHPC. As a result, the impedance matching between UHPC and the free space was improved and the electromagnetic waves were easier to enter UHPC, which was reflected by the reduction in the real part of the complex permittivity [43]. Contrarily, a conductive network was gradually formed with the increase in CB (2.0 vol.%), resulting in the decrease in the resistance of UHPC. Thus, the impedance matching was deteriorated and the electromagnetic wave was relatively difficult to enter UHPC. In this case, a slight difference between the real part of the complex permittivity of UHPC with 2.0 vol.% CB and the traditional UHPC was observed. With the continuous increase in CB (2.7 vol.%), the electromagnetic waves were more difficult to enter UHPC under the synergistic effects of the deteriorated impedance matching by the fully formed conductive network and the evident reflection of the electromagnetic waves in the free surface of the specimen. Therefore, the real part of the complex permittivity exhibited a significant increase, compared with the traditional UHPC.

The effect of CB on the imaginary part of the complex permittivity was further analyzed, as shown in Fig. 8(b). The imaginary part of the complex permittivity for UHPCs initially present an increasing trend with frequency, followed by a significant decrease or plateau stage based on the dosage of CB. The imaginary part of the complex permittivity for CB-UHPC-1.3-Perm initially increased from 0.5 at 2 GHz to 2.2 at 8 GHz, followed by a continuous decline to 1.25 at 18 GHz. However, the value of the imaginary part for CB-UHPC-2.0-Perm and CB-UHPC-2.7-Perm increased from 0.75 at 2 GHz to 2.3 and 2.9 at 9 GHz, respectively. Afterwards, it remained almost constant until 18 GHz. Thus, the imaginary part of the complex permittivity of UHPCs was significantly improved with the CB fraction. Meanwhile, the value of the imaginary part of the complex permittivity of UHPCs reinforced with CB was higher than that of the traditional UHPC in the full frequency range (2-18 GHz). These observations indicated that the addition of CB can significantly enhance the dielectric loss of UHPCs, based on Eq. (12).

Eventually, the effect of CB on the dielectric loss tangent was analyzed, as shown in Fig. 9. The dielectric loss tangent for UHPCs varied with frequency based on Eq. (7), which initially presented an increasing trend with frequency and followed by a significant decrease or plateau stage based on the CB dosage. The value of the dielectric loss tangent of CB-UHPC-1.3-Perm increased from 0.1 at 2 GHz to 0.58 at 8 GHz, followed by a decrease to 0.3 at 18 GHz. However, the value of the dielectric loss tangent for CB-UHPC-2.0-Perm and CB-UHPC-2.7-Perm increased from 0.18 at 2 GHz to 0.58 and 0.63 at 9 GHz, respectively. Afterwards, the value remained almost unchanged till 18 GHz. Overall, UHPCs mixed with CB exhibited an insignificant variation in 2-6.5 GHz frequency range, thus, indicating that it was uneconomical to improve the dielectric loss tangent of UHPCs in this frequency range by increasing the CB dosage.

Moreover, although the impedance matching of UHPCs was deteriorated on exceeding the CB content beyond 2.0 vol.%, however, the dielectric loss tangent was significantly improved with the CB content. As derived from Eq. 7, the addition of CB enhanced the dielectric loss (the imaginary part of the complex permittivity) of UHPCs more effectively than deteriorating the impedance matching. Correspondingly, the dielectric loss tangent was generally improved on incorporating CB. Meanwhile, values of the dielectric loss tangents of UHPCs incorporated with CB were much higher than that of the traditional UHPC in 2-18 GHz frequency range. As the loss tangent is used to reflect the capability of the medium to absorb/attenuate the electromagnetic wave, the observed findings indicate that the capability of UHPC to absorb/attenuate the electromagnetic wave can be significantly improved in 2-18 GHz frequency range on reinforcing with CB.

It is worth noting that obvious troughs existed in the real/imaginary part of the complex permittivity of UHPCs when the volumetric ratio of CB was below 1.3 vol.%. On the other hand, this phenomenon disappeared on exceeding the CB volumetric ratio beyond 2.0 vol.%. According to the fact that the complex permittivity is a material property, which is closely related to the state of electron in the material, the above observations could be attributed to the reason that the addition of CB changed the electrical properties of UHPC. Thus, the real/ imaginary part of the complex permittivity exhibited different variation regularities with the increase in the CB dosage, as shown in Fig. 8. Especially, compared with the electrical properties of UHPC under the low frequency, the increase in the CB content had a more significant effect on the electrical properties at the high frequency. Correspondingly,

the dielectric loss tangent varied with the frequency based on Eq. (7).

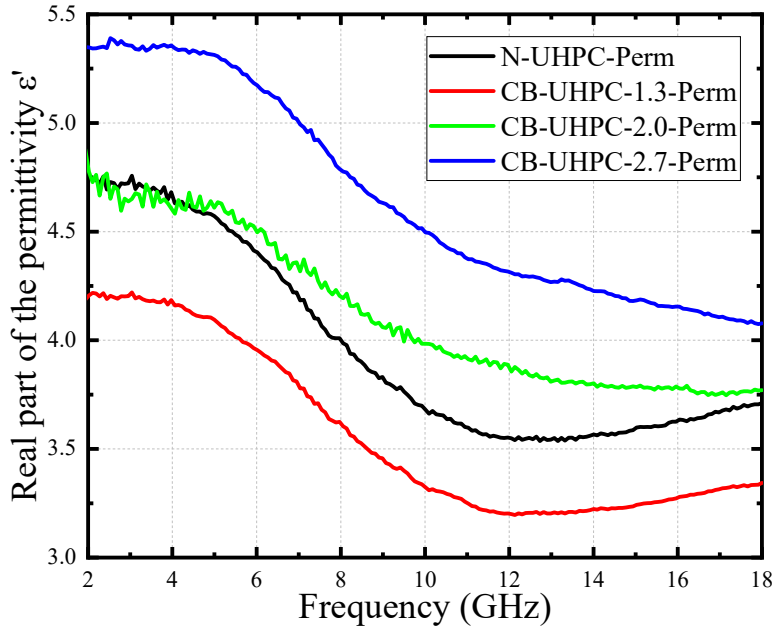

(a) The real part of the complex permittivity, ε'

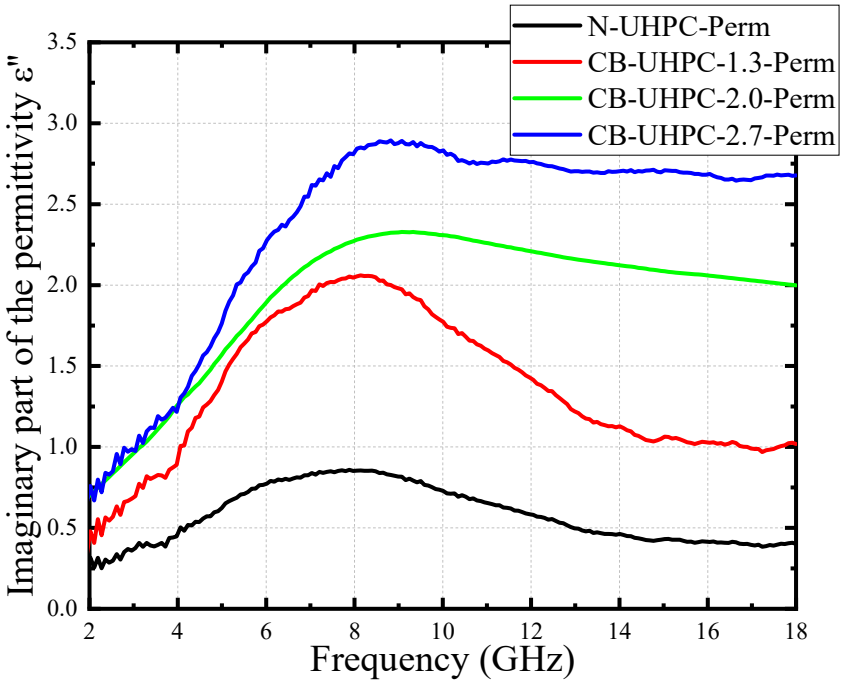

(b) The imaginary part of the complex permittivity, ε''

Fig. 8. The effect of CB on the complex permittivity of UHPCs.

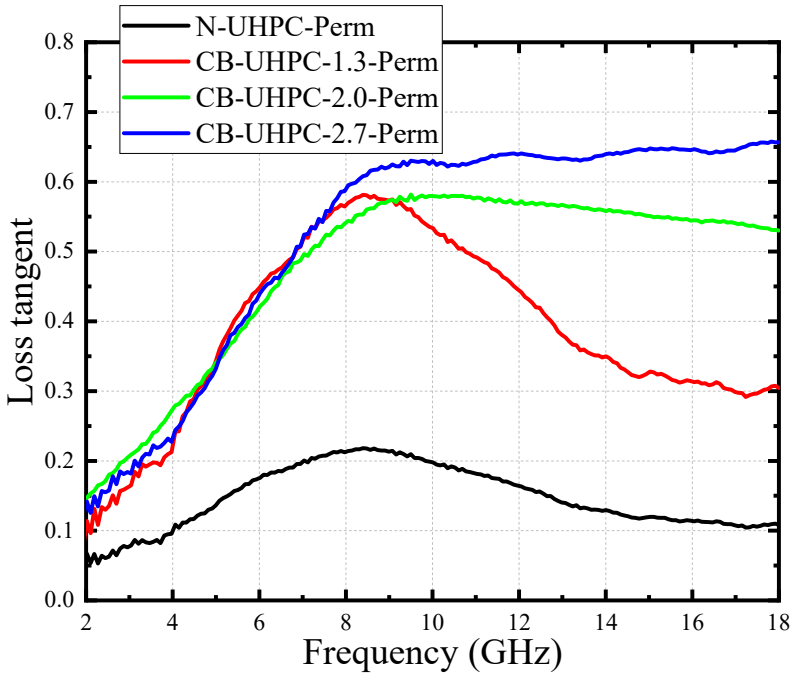

Fig. 9. Effect of CB on the dielectric loss tangent ($\tan(\delta_E)$) of UHPCs.

4.2.2 Effect of Carbon fiber

The effect of CF on the complex permittivity of UHPCs is shown in Fig. 10. The complex permittivity of the traditional UHPC has also been plotted in Fig. 10 for comparison. Fig. 10(a) shows the effect of CF on the real part of the complex permittivity. The real part of the complex permittivity of UHPCs incorporated with CF gradually decreased in 2-12 GHz frequency range, whereas a plateau stage was observed in 12-18 GHz range. In 2-12 GHz frequency range, the rate of decline in the real part of the complex permittivity increased with the CF dosage. Moreover, the value of the real part of the complex permittivity of UHPCs reinforced with CF was higher than that of the traditional UHPC in 2-18 GHz frequency range, along with a significantly increasing trend on enhancing the CF fraction. Similarly, based on Eq. (11), the observed phenomenon indicated that the impedance matching of UHPCs was severely deteriorated on adding CF, thus, making it difficult for the electromagnetic wave to enter UHPC.

The effect of CF on the imaginary part of the complex permittivity was further analyzed, as shown in Fig. 10(b). The imaginary part of the complex permittivity for UHPCs initially exhibited an increasing trend, followed by a significant decrease or plateau stage based on the CF dosage. For the specimen CF-UHPC-0.1-Perm, the value of the imaginary part of the complex permittivity increased from 1.4 at 2 GHz to 2.5 at 8 GHz, followed by a continuous decline to 1.6 at 18 GHz. A similar behavior was

observed for CF-UHPC-0.3-Perm, where the value of the imaginary part initially increased from 1.1 at 2 GHz to 3.8 at 7 GHz, which was subsequently decreased to 2.6 at 18 GHz. However, the imaginary part of the complex permittivity in the case of CF-UHPC-0.5-Perm demonstrated a continuous increase, followed by a plateau stage with an insignificant increment. This observation was due to the reason that the addition of CF altered the electrical properties of UHPC. However, unlike the effect of CB, the change in the CF content with the electrical properties of UHPC was more reflected on the imaginary part of the complex permittivity. Moreover, the values of the imaginary part of the complex permittivity of UHPCs incorporated with CF were much higher than that of the traditional UHPC in 2-18 GHz frequency range, and the values were significantly improved as a function of the CF content. Based on Eq. (12), the observed phenomenon indicated that the addition of CF could significantly enhance the dielectric loss of UHPCs, thus, benefitting their electromagnetic wave absorption capacity. However, the loss tangent of CF-UHPC-0.1-Perm had the largest value when the frequency was 2 GHz. This may be explained by the harmonic vibration effect occurring between the carbon fibres and the electromagnetic field as illustrated in literatures [44] since the behaviour resembles harmonic oscillators when the electromagnetic wave interacts with the composites [45]. Specifically, at a low frequency (2 GHz), the harmonic vibration between the CF in a low volumetric ratio (0.1 vol. %) and the electromagnetic field was stronger compared with the CF in a high low volumetric ratio, and the strong harmonic vibration further accelerated the dielectric loss reflected by the imaginary part.

Eventually, the effect of CF on the dielectric loss tangent is shown in Fig. 11. The trend was observed to be similar to the imaginary part of the complex permittivity (varied based on Eq. (7)). The value of the dielectric loss tangent of UHPC reinforced with 0.1 vol.% CF initially increased from 0.24 at 2 GHz to 0.55 at 8 GHz, with a subsequent decrease to 0.41 at 18 GHz. On increasing the CF dosage to 0.3 vol.%, the value of the dielectric loss tangent increased from 0.12 at 2 GHz to 0.61 at 8 GHz, followed by a gradual decline to 0.43 at 18 GHz. On the other hand, at 0.5 vol.% CF content, the value of the loss tangent increased from 0.12 at 2 GHz to 0.62 at 8 GHz and remained unchanged until 18 GHz. Overall, similar to the effect of CB, the capability of UHPCs to absorb/attenuate the electromagnetic wave could be significantly improved on adding CF, whereas it was uneconomical to improve the dielectric loss tangent of UHPCs in the frequency range of 2-7 GHz by increasing the CF dosage.

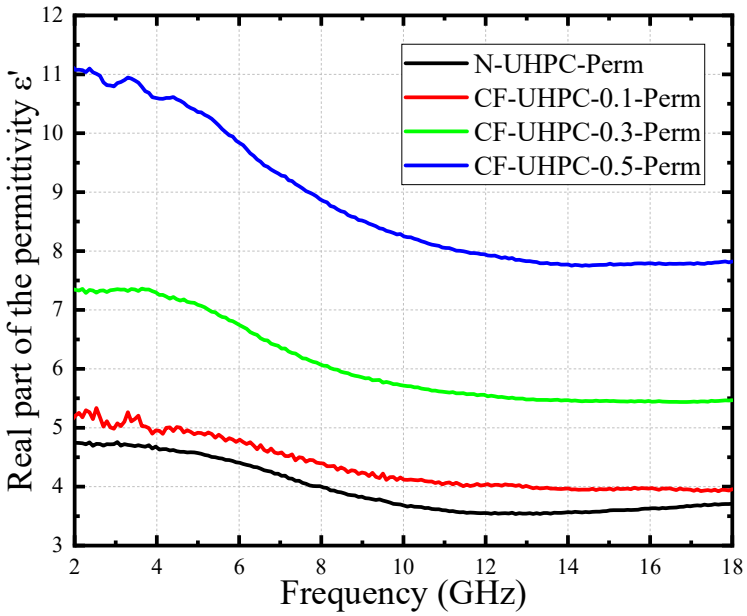

(a) The real part of the complex permittivity, ε'

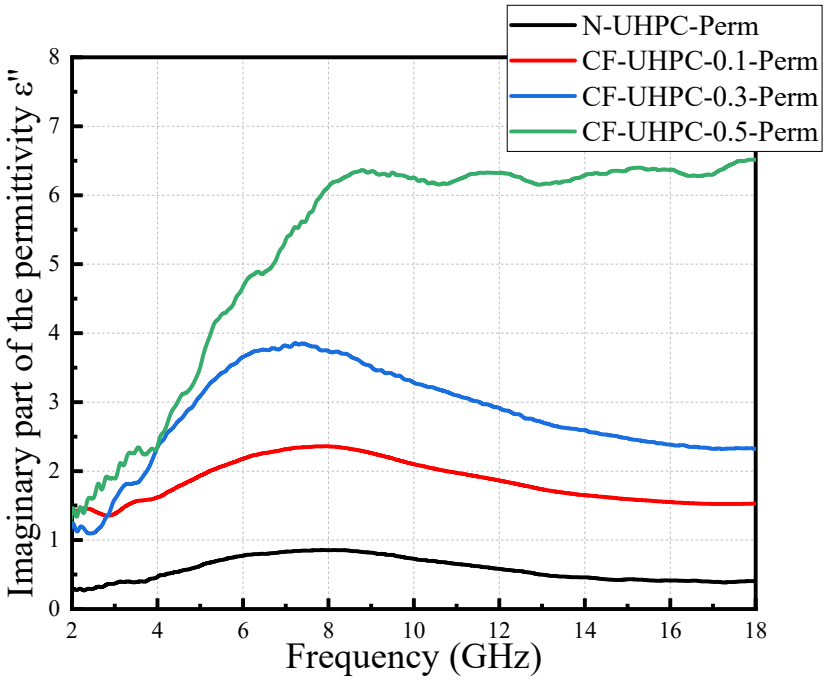

(b) The imaginary part of complex permittivity, ε''

Fig. 10. The effect of CF on the complex permittivity of UHPCs.

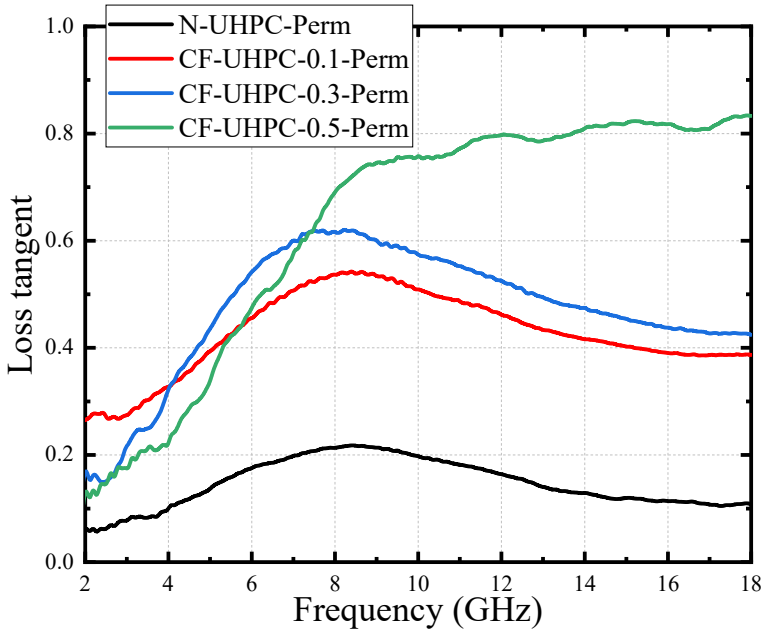

Fig. 11. The effect of CF on the dielectric loss tangent ($\tan(\delta_E)$) of UHPCs.

4.3 Effect of carbon black and carbon fiber on reflectivity of UHPCs

The reflectivity is the ultimate index to evaluate EWAP, and the effect of CB and CF on the reflectivity of UHPCs is presented in Figs. 12-15.

4.3.1 Effect of Carbon black

Fig. 12 demonstrates the effect of CB on the reflectivity of UHPCs. Four absorption peaks were observed for all UHPC samples as a function of frequency. In the traditional UPHC, the absorption peaks were observed at the higher reflectivity values as compared to UHPCs reinforced with CB. For instance, for the traditional UHPC, the four absorption peaks were -8.14 dB at 2.32 GHz, -7.98 dB at 9.36 GHz, -11.73 dB at 12.56 GHz and -13.76 dB at 18.0 GHz, whereas the effective bandwidth with reflectivity less than -10 dB was 0.8 GHz. On adding 1.3 vol.% CB, the effective bandwidth with reflectivity less than -10 dB was determined to be 2 GHz. On further increasing the CB dosage to 2.0 vol.%, the effective bandwidth with reflectivity less than -10 dB was increased to 2.8 GHz. UHPC mixed with 2.7 vol.% CB exhibited the absorption peaks -12.03 dB, -10.51 dB, -15.79 dB and -20.38 dB at 2 GHz, 9.6 GHz, 12.64 GHz and 18.0 GHz, respectively. Further, the effective bandwidth with reflectivity less than -10 dB was 6.96 GHz. Based on the observed findings, it could be concluded that the reflectivity of UHPCs was significantly decreased on adding CB, thus, reflecting an improved electromagnetic wave absorption performance.

The absorption peaks of UHPCs and the corresponding effective bandwidth values with reflectivity less than -10 dB are further summarized in Fig. 12(b). The reflectivity of P2 was higher than other peaks, whereas P4 exhibited the minimum reflectivity among the observed absorption peaks. The effect of increasing the CB dosage on the reflectivity of P1 was not regular, which revealed that the loss effect of CB on the electromagnetic wave at the low frequency was not positively correlated with the CB content. It may be attributed to the reason that there could exist a threshold of CB dosage at the low frequency. When the CB dosage was below the threshold, the effect of CB on the reflectivity at the low frequency was not regular. On the other hand, upon exceeding the threshold, the effect of CB on the reflectivity at the low frequency could be positively correlated with the CB dosage. However, the reflectivity of other peaks presented an obvious decline on increasing the CB dosage. Meanwhile, the effective bandwidth with reflectivity less than -10 dB significantly increased with the CB dosage, which indicated that the addition of CB enhanced the loss frequency range of the electromagnetic wave in 2-18 GHz frequency range. The fundamental contribution of CB towards improving the electromagnetic wave absorption properties of a double-layer microwave absorber was explained in literature [38], which is also relevant for this study. Based on this, it can be suggested that: (1) the electromagnetic wave is attenuated as the vibration of the conductive powder acting as a dipole is damped; (2) the electromagnetic wave is attenuated due to the multiple reflections; (3) the leakage-conductance effect between the conductive particles attenuates the electromagnetic wave.

Fig. 13(a) shows the microstructure of UHPC reinforced with 2.7 vol.% CB. CB was observed to be dispersed in the UHPC matrix, and the CB particles were noted to be adjacent to each other. Thus, it could be suggested that the distance between the CB particles decreased on increasing the CB dosage. Correspondingly, at a low dosage, the distance between the CB particles was too large to be conductive to the transmission of the electromagnetic wave, thus, further enhancing the reflectivity. On the other hand, a CB electronic network was formed in UHPC on enhancing the CB dosage, which was beneficial for the interaction and heat loss during the electromagnetic wave propagation in UHPC, as shown in Fig. 13(b) and (c).

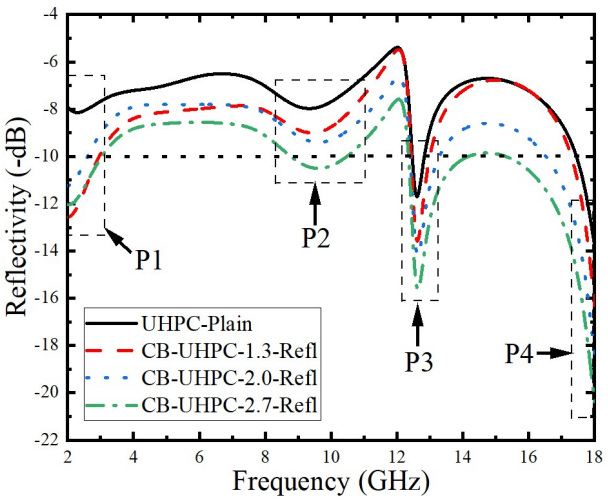

(a) Relationship of reflectivity and frequency (b) Peak reflectivity

Fig. 12. The effect of CB on the reflectivity of UHPCs.

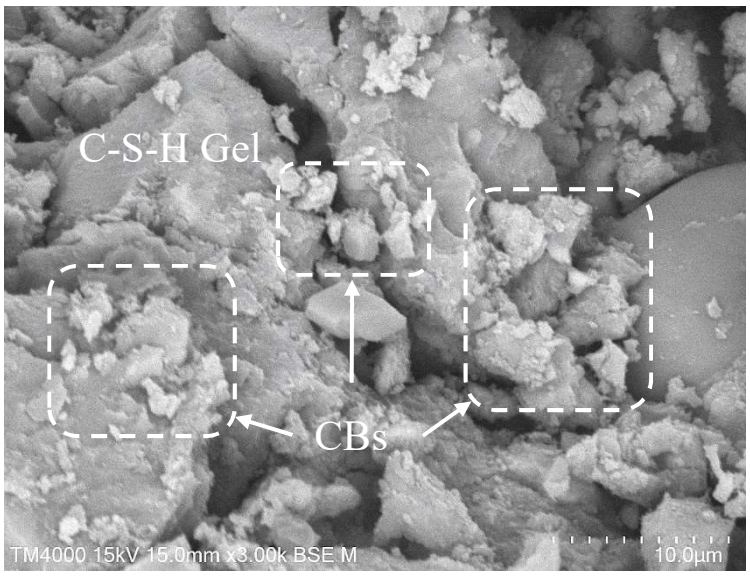

(a) The microstructure of CB-UHPC-2.7-Refl

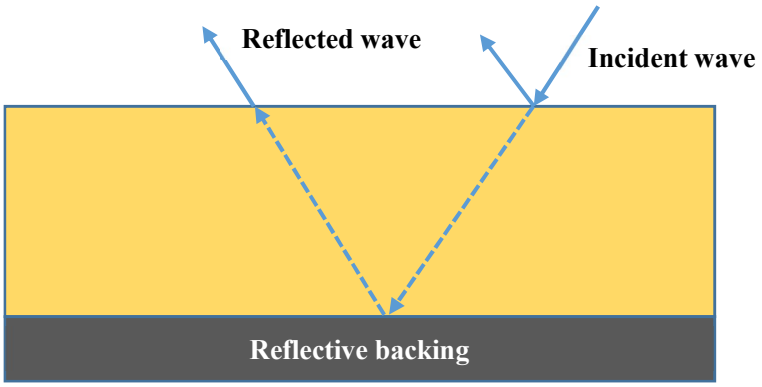

(b) The propagation of the electromagnetic wave in the traditional UHPC

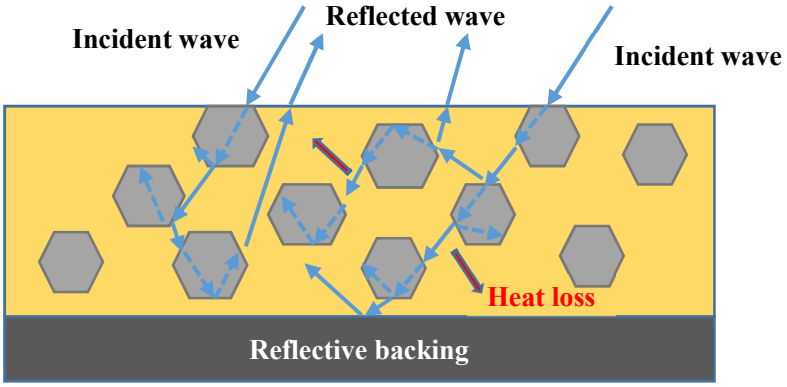

(c) The propagation of the electromagnetic wave in UHPC reinforced with a high dosage of CB

Fig. 13. The structural characteristics of UHPCs incorporated with CB.

4.3.2 Effect of Carbon fiber

The effect of CF on the reflectivity of UHPCs is presented in Fig. 14. Similar to CB, the UHPCs incorporated with CF exhibited four absorption peaks. The absorption peaks for UHPC incorporated with 0.1 vol.% CF were -13.48 dB at 2 GHz, -10.17 dB at 9.68 GHz, -17.13 dB at 12.64 GHz and -22.13 dB at 18 GHz. Correspondingly, the effective bandwidth with reflectivity less than -10 dB was observed to be 3.92 GHz. On increasing the CF dosage to 0.3 vol.%, the absorption peaks transformed to -13.22 dB at 2.08 GHz, -10.78 dB at 9.6 GHz, -18.76 dB at 12.64 GHz and -25.17 dB at 18 GHz, with the effective bandwidth with reflectivity less than -10 dB correspondingly increasing to 5.92 GHz. As the CF dosage was further increased to 0.5 vol.%, the absorption peaks decreased to -16.32 dB at 2.0 GHz, -12.41 dB at 9.6 GHz, -22.94 dB at 12.64 GHz and -30.69 dB at 18 GHz. Correspondingly, the effective bandwidth with reflectivity less than -10 dB increased to 8.32 GHz. Overall, the reflectivity of UHPCs could be significantly reduced on adding CF, thus, reflecting a marked improvement in EWAP of UHPCs

The absorption peaks of UHPCs and the corresponding effective bandwidth values with reflectivity less than -10 dB are further summarized in Fig. 14(b). The reflectivity of P2 was noted to be higher than other peaks, whereas P4 revealed the minimum reflectivity among the observed peaks. Overall, the reflectivity of the absorption peaks decreased on increasing the CF dosage, but the reflectivity peaks reinforced with 0.1 vol.% and 0.3 vol.% at P1 and P2 were similar. Like the effect of CB, this observation could also be attributed to the threshold of the CF dosage. The effect of CF on the reflectivity at the low frequency was similar when the CF dosage was smaller than the threshold.

Meanwhile, the effective bandwidth with reflectivity less than -10 dB also exhibited a significant increase with the CF content, which indicated that the CF addition enhanced the loss frequency range of the electromagnetic wave in 2-18 GHz frequency range. Correspondingly, the electromagnetic wave absorption of UHPCs was significantly improved on enhancing the CF content. The observed phenomenon was due to the conductive network formed by the dispersed CF phase in the UHPC matrix (Fig. 15(a)), which promoted the entry of the electromagnetic wave in UHPC. Meanwhile, the absorption and dissipation of the electromagnetic wave as other energy forms (such as heat) was accelerated during propagation through UHPC, as shown in Fig. 15(b).

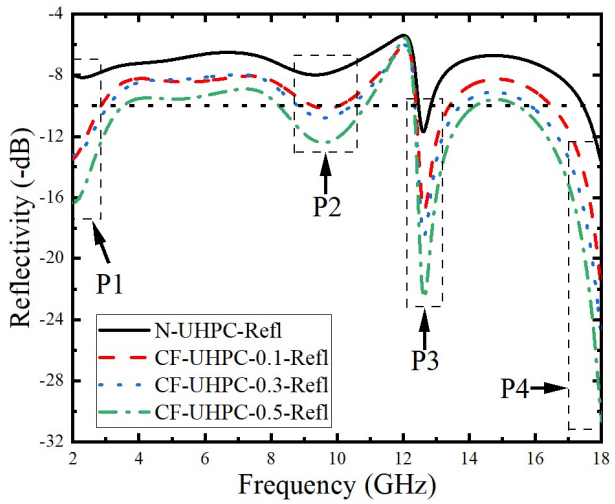

(a) Relationship between reflectivity and frequency

(b) Peak reflectivity

Fig. 14. The effect of CF on the reflectivity of UHPCs.

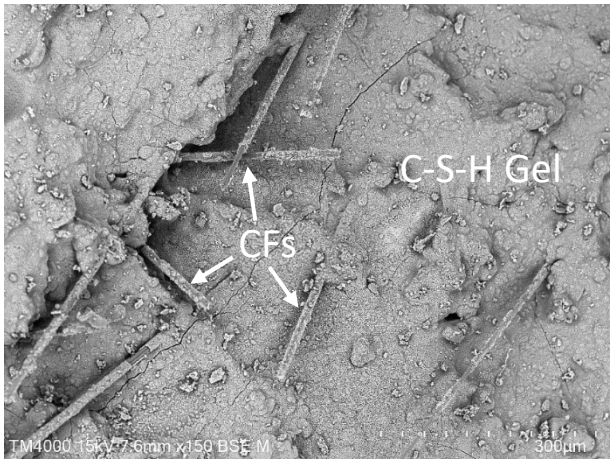

(a) The microstructure of CF-UHPC-0.5-Refl

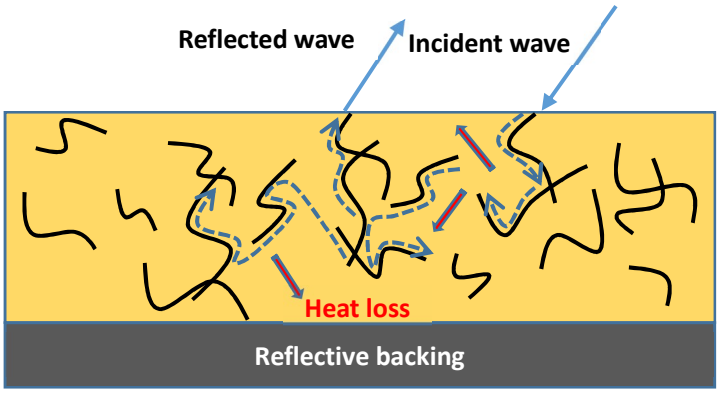

(b) The mechanism of propagation of the electromagnetic wave in UHPC reinforced with CF

Fig. 15. The structural characteristics of UHPC reinforced with CF.

4.4 Summary of the effect of CB and CF on compressive strength and reflectivity of UHPCs

Fig. 16 summarizes the effect of CB and CF on the compressive strength and reflectivity of UHPCs. As observed, the compressive strength significantly increased with the dosage of CB or CF. Specifically, on enhancing the CB content from 0 to 2.0 %, the compressive strength increased to 134.04 MPa, thus, indicating a 15.22% increase. On the other hand, an increment of 6.95% was observed as the dosage of CF was increased from 0 to 0.5 %. Meanwhile, the absorption peaks decreased with the CB dosage except P1, and the rate of decrease also increased with frequency. A similar trend was observed in the case of CF reinforcement. Thus, both CB and CF improved the compressive strength and reduced the reflectivity. In other words, UHPC with a high compressive strength presents a small reflectivity.

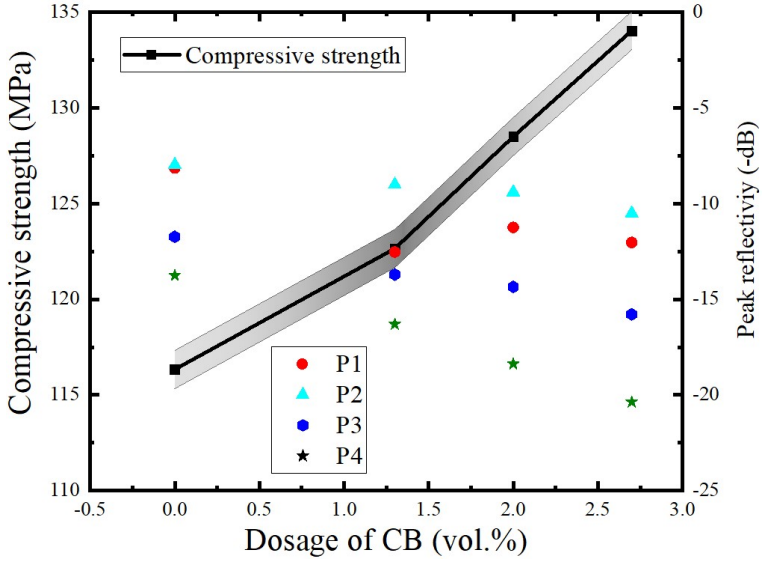

(a) Effect of CB on the compressive strength and reflectivity of UHPCs.

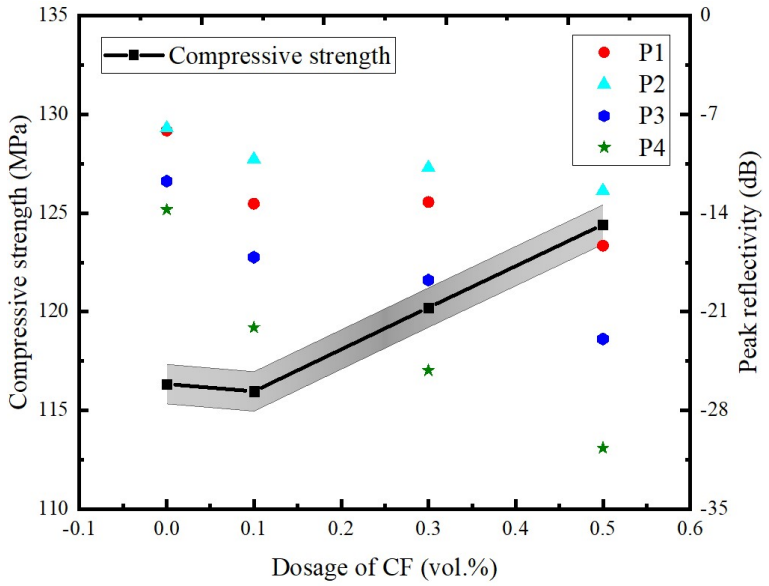

(b) Effect of CF on the compressive strength and reflectivity of UHPCs.

Fig. 16. Summary of the effect of CB and CF on the compressive strength and reflectivity of UHPCs.

4.5 Discussion

The normalization analysis was performed to further illustrate the effectiveness of CB and CF in improving EWAP of UHPC. The normalized dielectric loss tangent is defined as the ratio of the dielectric loss tangent of UHPCs reinforced with CB or CF to that of the traditional UHPC. On the other hand, the normalized reflectivity was defined as the ratio of the reflectivity of the traditional UHPC to that of UHPCs reinforced with CB or CF (as reflectivity is negative). Also, only the specimens which demonstrated the optimal EWAP in each test group (CB-UHPC-2.7-Perm, CB-UHPC-2.7-Relf, CF-UHPC-0.5-Perm and CF-UHPC-0.5-Relf) were analyzed.

The effect of CB and CF on the normalized dielectric loss tangent is compared in Fig. 17. The normalized dielectric loss tangents of CB-UHPC-2.7-Perm and CF-UHPC-0.5-Perm were observed to be very close to each other in 2-5 GHz frequency range, with both varying slightly in 2-3 GHz range. Further, the normalized dielectric loss tangent increased continuously on exceeding 5 GHz frequency. The rate of increment in the case of CF-UHPC-0.5-Perm was higher than CB-UHPC-2.7-Perm. Specifically, the largest value of the normalized dielectric loss tangent (7.28) was observed for CF-UHPC-0.5-Perm, which was reduced to 6.24 for CB-UHPC-2.7-Perm. The observed findings illustrated that the effectiveness of CF in improving the dielectric loss tangent of UHPCs was superior than CB, considering the fact that the CF dosage was much smaller than CB.

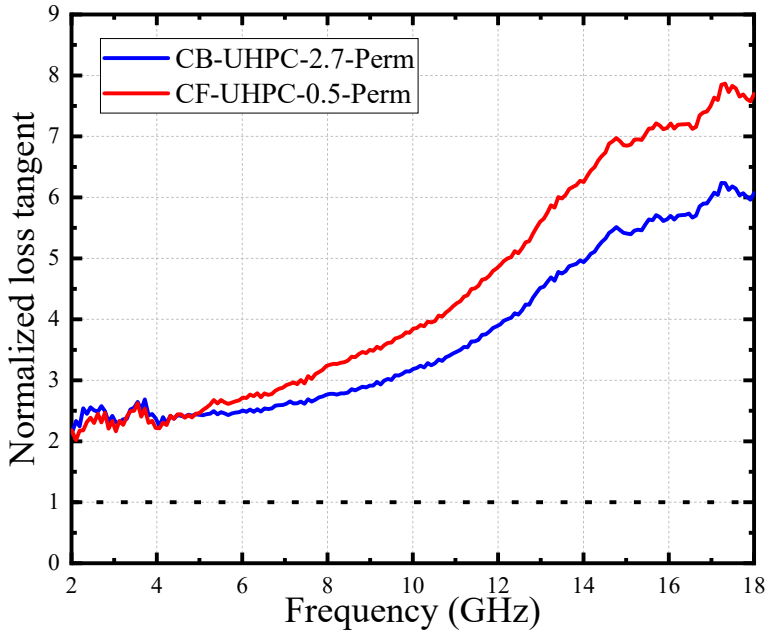

Fig. 17. The normalized loss tangent of CB-UHPC-2.7-Perm and CF-UHPC-0.5-Perm.

The effectiveness of CB and CF on the normalized reflectivity is presented in Fig. 18. The normalized reflectivity of CB-UHPC-2.7-Relf and CF-UHPC-0.5-Refl was below 1.0, which was smaller than that of the traditional UHPC. As compared to CF-UHPC-0.5-Relf, the normalized reflectivity of CB-UHPC-2.7-Relf was relatively stable in 2-18 GHz frequency range, and the corresponding smallest normalized reflectivity was 0.66. On the other hand, a dramatic variation was observed in CF-UHPC-0.5-Relf, especially at 12 GHz frequency. The smallest normalized reflectivity of CF-UHPC-0.5-Relf was 0.45, which was much smaller than that of CB-UHPC-2.7-Relf. Although the normalized reflectivity of CF-UHPC-0.5-Relf was much larger than that of CB-UHPC-2.7-Relf at 12 GHz frequency (and was very close to 1.0), however, it is smaller at other frequency values. This indicated that CF was more effective than CB in reducing the reflectivity of UHPCs, considering the fact that the CF dosage was much smaller than CB. This might be due to the reason that although CB was fully dispersed in the mortar matrix which could impart UHPC a certain conductivity, however, the inevitable presence of mortar between the CB particles hindered the propagation of the electromagnetic wave in UHPC to a certain extent. Moreover, the CF particles overlapped with each other in UHPC (as shown in Fig. 15), which allowed the propagation and absorption of the electromagnetic wave in UHPC, thus, enhancing the electromagnetic wave absorption efficiency.

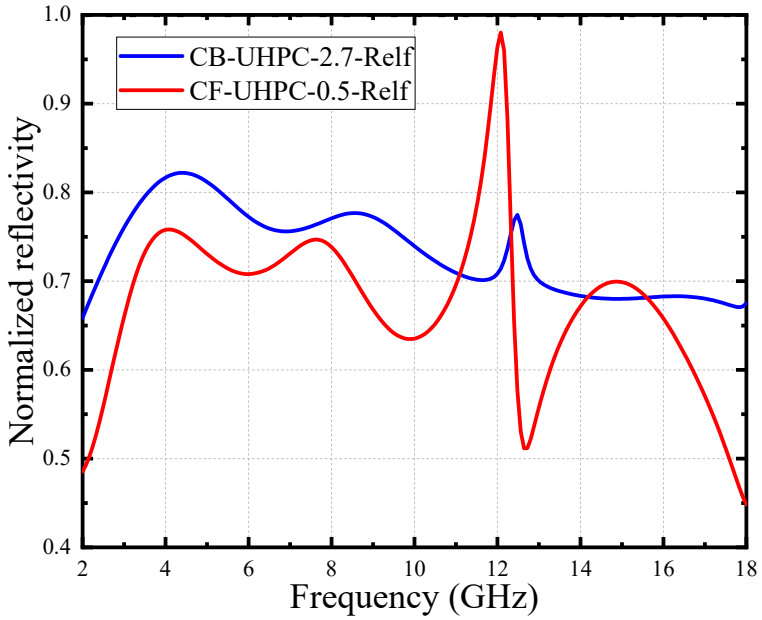

Fig. 18. The normalized reflectivity of CB-UHPC-2.7-Relf and CF-UHPC-0.5-Relf.

Eventually, the effective bandwidth with reflectivity less than -10 dB and compressive strength of UHPCs were compared with the typical cement-based composites reported in literature, as shown in Table 5. The effective bandwidth of UHPCs was much larger than a majority of the cement-based composites. In other words, EWAP of UHPCs was much superior than that the typical cement-based composites. Considering that the dosage of fillers in this study was similar to or less than that of the literature studies, EWAP can, thus, be improved further by enhancing the dosage of CB or CF. Moreover, the compressive strength of UHPCs in this study was a few times higher than a majority of the literature reported cement-based composites. Therefore, it could be concluded that UHPCs developed in this study possessed superior EWAP and excellent mechanical properties. Thus, it can be suggested that the safety of the protective engineering structures threatened by extreme loads including blast and penetration can be further improved by combining the superior EWAP and excellent mechanical properties of the developed UHPCs.

Table 5. The comparison of the electromagnetic wave absorption performance and compressive strength of the materials developed in this study with literature

Reference	Filler type	Content	Test frequency	Effective bandwidth	Compressive strength (MPa)
This study	Carbon black	2.7 vol.%	2-18 GHz	6.90 GHz	134.04
This study	Carbon fibre	0.5 vol.%	2-18 GHz	8.32 GHz	124.42
Xie et al. [18]	Helical carbon fiber	2 wt.%	2-18 GHz	13 GHz	30

He et al. [24]	Nano-Fe_3O_4	5 wt.%	8-18 GHz	9.5GHz	67.5
Li et al. [41]	Porous glass pellet	50 vol.%	1.7-18 GHz	7.47 GHz	11.41
Du et al. [46]	CBEB*	80 vol.%	2.6-8 GHz	3 GHz	3.75
Hu et al. [47]	Graphite	2 wt.%	8-18 GHz	4 GHz	16.9

**Note*: CBEB stands for carbon-coated expanded polystyrene beads. Effective bandwidth refers to the bandwidth with reflectivity less than -10 dB.

5. Conclusions

In order to develop innovative UHPCs with excellent EWAP and mechanical properties for protecting engineering structures against extreme loads (including blast and penetration), the effect of CB and CF on the compressive strength and EWAP of UHPCs was investigated in this study. The following conclusions can be drawn:

(1) The impedance matching of UHPCs was deteriorated on adding CF and it was also deteriorated on incorporating CB in excess of 2.7 vol.%, however, the dielectric loss tangent of UHPCs was significantly improved by adding CB or CF.

(2) Both CB and CF positively impacted the compressive strength and reduced the reflectivity of UHPCs. In comparison, CF was more effective in reducing reflectivity.

(3) Innovative UHPCs with excellent EWAP and mechanical properties can be developed by adding CB or CF to traditional UHPC.

Compliance with Ethical Standards

Funding: This study was funded by the National Natural Science Foundation of China (Grant No. 51908155 and 51978186).

Conflict of Interest: Author Shenchun Xu declares that he has no conflict of interest. Author Yekai Yang declares that he has no conflict of interest. Author Chengqing Wu declares that he has no conflict of interest.

Ethical approval: This article does not contain any studies with human participants or animals performed by any of the authors.

References

[1] Guan, H., Liu, S., Duan, Y., & Cheng, J. (2006). Cement based electromagnetic shielding and absorbing building materials. Cement and Concrete Composites, 28(5), 468-474.

[2] Roller, C., Mayrhofer, C., Riedel, W., & Thoma, K. (2013). Residual load capacity of exposed and hardened concrete columns under explosion loads. Engineering structures, 55, 66-72.

[3] Ha, J. H., Yi, N. H., Choi, J. K., & Kim, J. H. J. (2011). Experimental study on hybrid CFRP-PU strengthening effect on RC panels under blast loading. Composite Structures, 93(8), 2070-2082.

[4] Yamaguchi, M., Murakami, K., Takeda, K., & Mitsui, Y. (2011). Blast resistance of double-layered reinforced concrete slabs composed of precast thin plates. Journal of Advanced Concrete Technology, 9(2), 177-191.

[5] Graybeal, B.A. (2006). Material property characterization of ultra-high performance concrete. No. FHWA-HRT-06-103. United States: Federal Highway Administration. Office of Infrastructure Research and Development.

[6] Su, Y., Li, J., Wu, C., Wu, P., & Li, Z. X. (2016). Effects of steel fibres on dynamic strength of UHPC. Construction and Building Materials, 114, 708-718.

[7] Su, Y., Li, J., Wu, C., Wu, P., & Li, Z. X. (2016). Influences of nano-particles on dynamic strength of ultra-high performance concrete. Composites Part B: Engineering, 91, 595-609.

[8] Van Mier, J.G.M., Ruiz, G., Andrade, C., & Yu, R.C. (2013). Properties of ultra high performance concrete (UHPC) in tension at high strain rates. Proceedings of the FraMCoS-8.

[9] Su, Y., Wu, C., Li, J., Li, Z. X., & Li, W. (2017). Development of novel ultra-high performance concrete: From material to structure. Construction and Building Materials, 135, 517-528.

[10] Wu, C., Li, J., & Su, Y. (2018). Development of Ultra-High Performance Concrete against Blasts (SBN: 9780081024959), Woodhead Publishing, SBN: 9780081024959 https://www.elsevier.com/books/development-of-ultra-high-performanceconcrete-against-blasts/wu/978-0-08-102495-9.

[11] Liu, J., Wu, C., & Chen, X. (2017). Numerical study of ultra-high performance concrete under non-deformable projectile penetration. Construction and Building Materials, 135, 447-458.

[12] Liu, J., Wu, C., Li, J., Su, Y., Shao, R., Liu, Z., & Chen, G. (2017). Experimental and numerical study of reactive powder concrete reinforced with steel wire mesh against projectile penetration. International Journal of Impact Engineering, 109, 131-149.

[13] Liu, J., Wu, C., Su, Y., Li, J., Shao, R., Chen, G., & Liu, Z. (2018). Experimental and numerical studies of ultra-high performance concrete targets against high-velocity projectile impacts. Engineering Structures, 173, 166-179.

[14] Wu, H., Fang, Q., Chen, X. W., Gong, Z. M., & Liu, J. Z. (2015). Projectile penetration of ultra-high performance cement based composites at 510–1320 m/s. Construction and Building Materials, 74, 188-200.

[15] Wang, Z., Wang, Z., & Ning, M. (2020). Optimization of electromagnetic wave absorption bandwidth of cement-based composites with doped expanded perlite. Construction and Building Materials, 259, 119863.

[16] Zhang, W., Zheng, Q., Wang, D., Yu, X., & Han, B. (2019). Electromagnetic properties and mechanisms of multiwalled carbon nanotubes modified cementitious composites. Construction and Building Materials, 208, 427-443.

[17] Li, Z., Dong, S., Wang, X., Yu, X., & Han, B. (2020). Electromagnetic wave-absorbing property and mechanism of cementitious composites with different types of nano titanium dioxide. Journal of Materials in Civil Engineering, 32(5), 04020073.

[18] Xie, S., Ji, Z., Li, B., Zhu, L., & Wang, J. (2018). Electromagnetic wave absorption properties of helical carbon fibers and expanded glass beads filled cement-based composites. Composites Part A: Applied Science and Manufacturing, 114, 360-367.

[19] Cui, X., Sun, S., Han, B., Yu, X., Ouyang, J., Zeng, S., & Ou, J. (2017). Mechanical, thermal and electromagnetic properties of nanographite platelets modified cementitious composites. Composites Part A: Applied Science and Manufacturing, 93, 49-58.

[20] Wang, Z. J., Li, K. Z., & Wang, C. (2014). Freezing–thawing effects on electromagnetic wave reflectivity of carbon fiber cement based composites. Construction and Building materials, 64, 288-292.

[21] Wang, B., Guo, Z., Han, Y., & Zhang, T. (2013). Electromagnetic wave absorbing properties of multi-walled carbon nanotube/cement composites. Construction and building materials, 46, 98-103.

[22] Dai, Y., Sun, M., Liu, C., & Li, Z. (2010). Electromagnetic wave absorbing characteristics of carbon black cement-based composites. Cement and Concrete Composites, 32(7), 508-513.

[23] Wang, D., Yang, P., Hou, P., Zhang, L., Zhang, X., Zhou, Z., Xie, N., Huang, S., & Cheng, X. (2017). Cement-based composites endowed with novel functions through controlling interface microstructure from Fe3O4@ SiO2 nanoparticles. Cement and Concrete Composites, 80, 268-276.

[24] He, Y., Lu, L., Sun, K., Wang, F., & Hu, S. (2018). Electromagnetic wave absorbing cement-based

composite using Nano-Fe3O4 magnetic fluid as absorber. Cement and Concrete Composites, 92, 1-6.

[25] Guan, B., Ding, D., Wang, L., Wu, J., & Xiong, R. (2017). The electromagnetic wave absorbing properties of cement-based composites using natural magnetite powders as absorber. Materials Research Express, 4(5), 056103.

[26] Wang, Z., Zhang, T., & Zhou, L. (2016). Investigation on electromagnetic and microwave absorption properties of copper slag-filled cement mortar. Cement and Concrete Composites, 74, 174-181.

[27] Wen, B., Zhao, J., Duan, Y., Zhang, X., Zhao, Y., Dong, C., Liu, S., & Li, T. (2006). Electromagnetic wave absorption properties of carbon powder from catalysed carbon black in X and Ku bands. Journal of physics D: Applied Physics, 39(9), 1960.

[28] Gong, H., Li, Z., Zhang, Y., & Fan, R. (2009). Piezoelectric and dielectric behavior of 0-3 cement-based composites mixed with carbon black. Journal of the European Ceramic Society, 29(10), 2013-2019.

[29] Huang, S., Li, X., Liu, F., Chang, J., Xu, D., & Cheng, X. (2009). Effect of carbon black on properties of 0–3 piezoelectric ceramic/cement composites. Current Applied Physics, 9(6), 1191-1194.

[30] Chan, W. W. J., & Wu, C. M. L. (2000). Durability of concrete with high cement replacement. Cement and Concrete Research, 30(6), 865-879.

[31] Gu, J., Li, Y., Liang, C., Tang, Y., Tang, L., Zhang, Y., Kong, J., Liu, H., & Guo, Z. (2018). Synchronously improved dielectric and mechanical properties of wave-transparent laminated composites combined with outstanding thermal stability by incorporating iysozyme/POSS functionalized PBO fibers. Journal of Materials Chemistry C, 6(28), 7652-7660.

[32] Xie, S., Ji, Z., Yang, Y., Hou, G., & Wang, J. (2016). Electromagnetic wave absorption enhancement of carbon black/gypsum based composites filled with expanded perlite. Composites Part B: Engineering, 106, 10-19.

[33] Rhim, H. C., & Buyukozturk, O. (1998). Electromagnetic properties of concrete at microwave frequency range. Materials Journal, 95(3), 262-271.

[34] Büyüköztürk, O., & Rhim, H. C. (1993, June). Electromagnetic properties of concrete for nondestructive testing. In Proceedings of the International Conference on Nondestructive Testing

of Concrete in the Infrastructure (pp. 83-92). Society for Experimental Mechanics Dearborn, Michigan.

[35] Zhang, X., & Xi, Z. (2003). Building electromagnetic wave absorber and its application on the environment protection of habitation. Journal of Building Materials, 01, 72-75.

[36] Zheng, C., Li, J., Zhao, N., & Guo, X. (2004). Design and Application of Microwave Absorbing Materials. Aerospace Materials & Technology, 05, 1-5.

[37] Guru, B. S., & Hiziroglu, H. R. (2009). Electromagnetic field theory fundamentals. Cambridge university press, 351-416.

[38] Wang, M., Duan, Y., Liu, S., Li, X., & Ji, Z. (2009). Absorption properties of carbonyl-iron/carbon black double-layer microwave absorbers. Journal of Magnetism and Magnetic Materials, 321(20), 3442-3446

[39] Zhang, Q., Tian, Z., Tang, W., Tang, N., Zhao, H., & Lin, H. (2019). Study of attenuation characteristics of electromagnetic waves in multilayer plasma slabs. Journal of Applied Physics, 125(9), 094902.

[40] Zhang, W., Xu, H., Song, Z., Han, X., Wei, X., Wu, X., & Li, Y. (2019). Study on attenuation characteristics of electromagnetic waves in plasma-superimposed artificial wave vector metasurface structure. Journal of Physics D: Applied Physics, 53(6), 065204.

[41] Li, B., Duan, Y., Zhang, Y., & Liu S. (2011). Electromagnetic wave absorption properties of cement-based composites filled with porous materials. Materials & Design, 32(5), 3017-3020.

[42] Li, B., Duan, Y., Zhang, Y., & Liu S. (2011). The electromagnetic characteristics of fly ash and absorbing properties of cement-based composites using fly ash as cement replacement. Construction and Building materials, 27(1), 184-188.

[43] Leyva, M. E., Barra, G. M., Moreira, A. C., Soares, B. G., & Khastgir, D. (2003). Electric, dielectric, and dynamic mechanical behavior of carbon black/styrene‐butadiene‐styrene composites. Journal of Polymer Science Part B: Polymer Physics, 41(23), 2983-2997.

[44] Kezhi, L., Chuang, W., Hejun, L., Fa, L., & Dangshe, H. (2007). Reflectivity of carbon-fiber-reinforced cement-based composites against electromagnetic waves. Rare Metal Materials and Engineering, 36(10), 1702.

[45] Zhao, N., Zou, T., Shi, C., Li, J., & Guo, W. (2006). Microwave absorbing properties of activated carbon-fiber felt screens (vertical-arranged carbon fibers)/epoxy resin composites. Materials

Science and Engineering: B, 127(2-3), 207-211.

[46] Du, J., Liu, S., & Guan, H. (2006). Research on the absorbing characteristics of cement matrix composites filled with carbon black-coated expanded polystyrene beads. Advances in cement research, 18(4), 161-164.

[47] Hu, S. G., Tian, K., & Ding, Q. J. (2008, November). Design and test of new cement-based microwave absorbing materials. In 8th International Symposium on Antennas, Propagation and EM Theory (pp. 956-959). IEEE.